

The Angular Dependence of the Critical Current of BaCeO₃ Doped YBa₂Cu₃O_{6+x} Thin Films

M. Malmivirta, L.D. Yao, S. Inkinen, H. Huhtinen, H. Palonen, R. Jha, V. P. S. Awana, S. van Dijken and P. Paturi

Abstract—The angular dependencies of the critical current of BaCeO₃ (BCO) doped YBa₂Cu₃O_{6+x} (YBCO) thin films grown with pulsed laser deposition (PLD) on SrTiO₃ (001) were systematically investigated. The BCO concentration in the YBCO matrix was varied between 0 – 8 wt.%. Transmission electron microscopy confirmed that the 4 % BCO containing sample has point-like, partly agglomerated BCO particles with diameter of 2.5 nm. The dopant degrades the crystal quality of YBCO but improves its in-field current carrying performance especially at low temperatures. The BCO addition affects the angular dependence of the critical current by broadening the $B||ab$ -axis peak of YBCO but no c -axis peak is seen, which is contrary to BaZrO₃ doped films made by PLD. Although the particles are point-like, it is found that a model featuring only isotropic pinning centers is not sufficient to describe the angular dependence of the samples where $B||ab$ -axis of YBCO.

Index Terms—YBCO thin films, BaCeO₃ doping, Angular dependence of critical current, Pulsed laser deposition

I. INTRODUCTION

DOPING YBa₂Cu₃O_{6+x} (YBCO) with a non-superconducting second phase has been used as a method to improve the in-field performance. In a simple model, the second phase additions create non-superconducting areas that pin vortices. In many cases, the form of the addition in the YBCO matrix can give a hint about $J_c(\theta)$, the angular dependence of critical current. Correlated nanorods are formed *e.g.* when BaZrO₃ (BZO) doped YBCO is grown by pulsed laser deposition (PLD) [1]–[3]. The rods are seen as a c -axis peak in the angular dependence of the critical current. However, when grown by chemical solution deposition (CSD), BZO forms non-coherent non-correlated defects [4]–[6]. On the other hand, BaCeO₃ (BCO), when grown by PLD, forms non-columnar, epitaxial defects according to X-ray measurements [7]. The small difference between the lattice parameters of BZO and BCO, 4.2 Å and 4.4 Å respectively,

Manuscript received November 25, 2014. This work was supported by the Jenny and Antti Wihuri Foundation.

M. Malmivirta, H. Huhtinen, H. Palonen, and P. Paturi are with the Wihuri Physical Laboratory, Department of Physics and Astronomy, University of Turku, FI-20014 Turku, Finland, (e-mail: mika.malmivirta@utu.fi).

M. Malmivirta is also with the University of Turku Graduate School (UTUGS), University of Turku, FI-20014, Finland.

L.D. Yao, S. Inkinen and S. van Dijken are with the NanoSpin, Department of Applied Physics, Aalto University, School of Science, P.O. Box 15100, FI-00076, Aalto, Finland.

R. Jha and V. P. S. Awana are with the Superconductivity Division, National Physical Laboratory (CSIR), New Delhi 110012, India.

suggests that the lattice parameters can affect the shape of the nanoparticle.

Doping also affects the effective anisotropy, *i.e.* the amount that J_c changes as the direction of the magnetic field is varied. Also, the intrinsic anisotropy of YBCO can be modified by doping [6], [8]. The effect of the anisotropy on J_c can be described with Blatter scaling but the model describes only pinning due to isotropic pinning centers. The critical current is calculated by scaling the magnetic field as a function of the angle between the field and the YBCO lattice. According to the model, J_c can be described as [9], [10]

$$J_{c,iso}(\theta) = J_{c,0} [\cos^2(\theta) + \gamma^{-2} \sin^2(\theta)]^{-1/2}, \quad (1)$$

where θ is the angle between the magnetic field and YBCO c -axis, γ the anisotropy parameter and $J_{c,0}$ a scaling parameter, in practice J_c at $\theta = 0^\circ$. In addition to this, improved models for $J_c(\theta)$, like the vortex path model, can be used (see [11]–[14]).

In this paper, the angular dependence of the critical current of a concentration series of BCO doped YBCO thin films grown by PLD is discussed. The samples are analyzed with X-ray diffraction and transmission electron microscopy in addition to measuring the basic superconducting properties. The correlations between structural and superconducting properties are discussed in terms of isotropic and anisotropic flux pinning models.

II. EXPERIMENTAL DETAILS

The samples, consisting of YBCO and 0 – 8 wt.% of BCO, were grown with a pulsed laser deposition system on 5 mm × 5 mm SrTiO₃ (100) substrates. The BCO content in the targets was varied with 2 % steps. More details of the target preparation can be found in [7]. All the samples were deposited at 750 °C and after that oxygenated at 700 °C for 10 minutes in atmospheric pressure of oxygen. With 1500 pulses the average film thickness was 220 nm. More details on the ablation procedure can be found in [8].

The crystal structure of the samples was determined using an X-ray diffractometer (Philips X’pert Pro with Schulz texture goniometer). To assure the purity of the films, $\theta - 2\theta$ scans with $\psi = 0$ were measured between 20° – 110°. Also, accurate $\theta - 2\theta$ scans and rocking curves of YBCO (005) were used to determine the quality of the samples. The twinning of the films was determined from $2\theta - \phi$ scans of YBCO (212) peak (as in [15]) and crystalline orientation determined by scanning

the (102) peak with a - and c -axis configuration. To examine the growth of BCO, $\theta - 2\theta$ scans of BCO (002) and $2\theta - \phi$ of BCO (110) were taken. The cross-sectional morphology of the 4 % BCO doped YBCO film was analyzed using a JEOL 2200FS transmission electron microscope (TEM) with double Cs correctors, operated at 200 keV. The wedging cross-sectional TEM specimen was prepared by a modified mechanical polishing method: a Si/film/Si sandwich structure is firstly glued by epoxy after which it is cut into thin slices. After that, the thin slices are ground and polished by a MultiPrep polishing system (Allied High Tech products, Inc.), and finally milled by Ar ion polishing system (Model 691 PIPS, Gatan Inc.) available for TEM observations. BCO particle size distribution was analyzed by ImageJ software.

The basic characterization of the superconducting properties of the samples was done with a Quantum Design's Physical Property Measurement System (PPMS) with the ACMS-option. The critical temperature T_c was defined as the onset temperature of the in-phase component of the AC-magnetization. The critical current as a function of magnetic field was determined from the DC-magnetization of the sample in the field between -8 and 8 T at 10 K and 77 K using the Bean formula [16]. By using the Horizontal Rotator option of the PPMS the angular dependencies of the critical currents were measured. Each sample was patterned with a $50 \mu\text{m}$ wide current stripe using wet chemical etching and measured in maximum Lorentz force configuration. The angle was scanned with 3° steps between 0° and 360° at temperatures of 10 , 40 , 70 and 77 K in magnetic fields of 1 T and 6 T. The voltage along the current stripe was measured as a function of applied current at each angle step. The critical current was taken as the current at which the electric field of $215 \mu\text{V}/\text{cm}$ was induced. The voltage limit is higher than usual due to the small size of the samples, but it does not change the shape of the $J_c(\theta)$ curves [17].

III. RESULTS AND DISCUSSION

A. Structural Properties

In the $\theta - 2\theta$ scans of the samples, the full width at half maximum (FWHM) values of YBCO (005) peaks show an increase from 0.18° to 0.28° as the BCO concentration increases (Table I). Also the FWHM of the rocking curves (rc) of the same peak broadens from 0.15° to 0.39° . That is to say, both strained areas and the slight out-of-plane orientation of YBCO increases with increasing BCO concentration. In addition, the c -axis of YBCO increases with concentration, being 11.679 \AA with 0% sample and 11.716 \AA with the 8% sample. The correlation length (calculated as presented in [18]) decreases with increasing concentration from 28 nm to 11 nm of the 8% doped sample. The correlation length describes the distance over which atomic positions are correlated. The trends noted here are somewhat clearer than what has been earlier observed [7]. According to $2\theta - \phi$ scans of YBCO (212)/(122) peak set the crystal structures of the samples are biaxially twinned. Moreover, according to the $2\theta - \phi$ scans of YBCO (102) peaks, no a -axis oriented grains were formed.

TABLE I
THE BASIC STRUCTURAL AND SUPERCONDUCTING PROPERTIES OF THE SAMPLES.

BCO concentration	0 wt.%	2 wt.%	4 wt.%	6 wt.%	8 wt.%
FWHM (005) ($^\circ$)	0.17	0.19	0.23	0.24	0.28
FWHM rc(005) ($^\circ$)	0.15	0.19	0.21	0.34	0.38
c -axis (\AA)	11.679	11.685	11.693	11.704	11.716
r_c (nm)	28	23	20	13	11
T_c (K)	88.1	87.5	87.1	85.8	83.0
ΔT_c (K)	1.6	1.3	2.1	2.3	3.5
$T = 10 \text{ K}$					
$J_c(0 \text{ T})$ (MA/cm 2)	54	53	40	28	22
$J_c(3 \text{ T})$ (MA/cm 2)	7.3	8.9	7.9	6.5	5.8
B^* (mT)	81	95	89	116	127
α	0.44	0.42	0.38	0.36	0.33
$T = 77 \text{ K}$					
$J_c(0 \text{ T})$ (MA/cm 2)	3.5	3.4	2.0	0.75	0.20
B^* (mT)	5.8	6.6	5.1	4.6	2.7
α	0.25	0.23	0.23	0.25	0.29

The only difference of the $\theta - 2\theta$ scans between doped and undoped samples is a rise of intensity at a broad angular range around the 2θ value of 41° corresponding to (002) peak of BCO. From that the diameter of BCO particle has been calculated to be approximately 20 \AA [7]. In addition, because no other peaks of BCO were seen, it can be concluded that BCO has grown epitaxially. Due to the epitaxiality of BCO, the distortion in the YBCO lattice is smaller than with randomly oriented BCO particles. The epitaxiality is not the case for example in CSD grown films [6], where a large fraction of the BCO particles have random orientation. Due to the small size of the BCO particles, the BCO peaks (002) and (110) could not be analyzed.

The growth of BCO as very small particles suggested by XRD results is supported by the cross sectional morphology of the $4 \text{ wt.}\%$ doped sample imaged by bright field TEM (Fig. 1 (a)). The grown BCO particles are point-like with a mean diameter of $2.5 \pm 0.7 \text{ nm}$ (Fig. 1 (b)), which is considerably smaller than BCO nanodots prepared by CSD [6], about 50 nm , and also smaller than the diameter of BZO nanorods in YBCO grown by PLD [19], [20]. The BCO particles are dispersive but in some local areas they are clustered into lines in the direction of the ab -planes. We have also seen that with higher BCO concentration the particles become more aggregative. In addition to the nanodots, the sample contains a lot of stacking faults in the $\{00l\}$ plane. They can be seen in the TEM image as line type contrasts along the ab -plane. All in all, the distortion caused by BCO can also be clearly seen in TEM images.

B. Magnetic Properties

The magnetically determined critical temperatures decrease from 88.1 K to 83.0 K with increasing concentration (Table I). With increasing concentration also the width of the transition increases almost systematically from 1.6 K for the undoped to

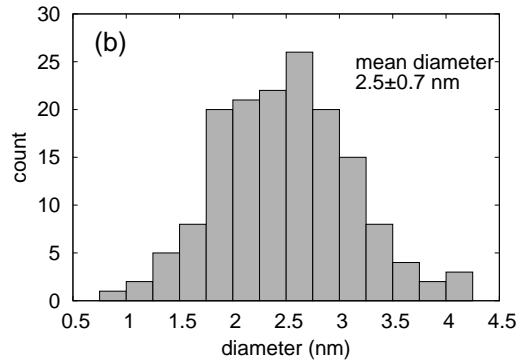
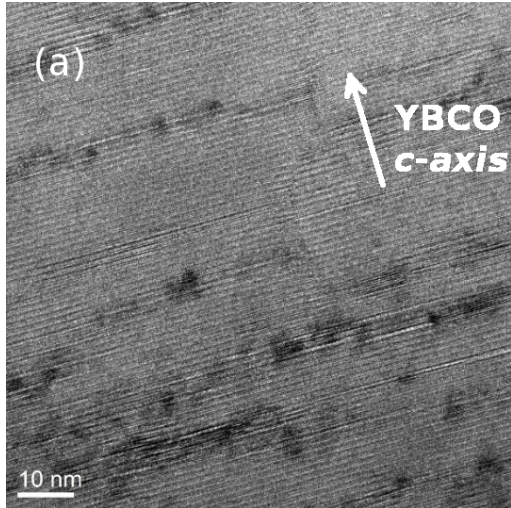


Fig. 1. (a) The cross sectional TEM image of the 4 % BCO doped sample and (b) the size distribution of the BCO particles in the same sample.

3.5 K for the 8 % doped sample. The magnetically determined critical currents in the case $B \parallel c$ -axis of YBCO show also a clear dependence on BCO concentration. At 10 K the self-field J_c deteriorates from the undoped sample value of 54 MA/cm² to 22 MA/cm² of the 8 % sample. However, the J_c at the field of 3 T is highest with the 2 % and 4 % doped samples. At 77 K 0 T the trend is pretty similar: J_c decreases with increasing concentration being between 3.5 MA/cm² and 0.20 MA/cm². The trends on T_c and J_c are similar to those noted before [7], [21].

The samples behave differently with respect to concentration if we look at the degradation rate of the J_c *i.e.* α in $J_c \propto B^{-\alpha}$. At 10 K the 8 % sample has the lowest α of 0.33 (Table I), which is about 0.1 larger than for the BZO doped YBCO samples [3], [20]. At 77 K the pinning capability of BCO particles is deteriorated: the highest α is achieved with high BCO concentration.

The effect of BCO is also seen in the accommodation field B^* at which $J_c = 0.9J_c(0 \text{ T})$. At 10 K, the higher the BCO concentration the higher is B^* (increases almost linearly from 81 mT to 127 mT, see Table I). The behavior is roughly similar to the previously made samples [7]. At 77 K, however, the accommodation field decreases with increasing concentration.

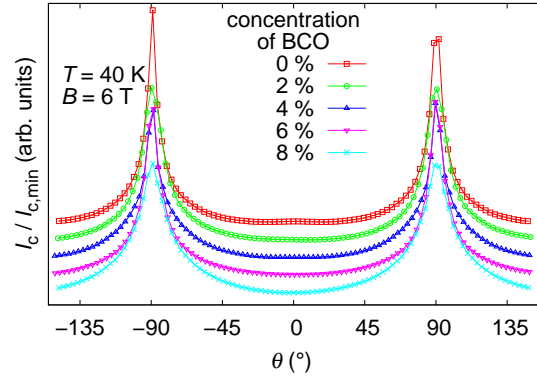


Fig. 2. The angular dependence of critical current as a function of angle between magnetic field and YBCO c -axis, each curve scaled by its minimum value and shifted for clarity. The order of the curves at $\theta = 0^\circ$ is the same as in the legend.

The value drops from 5.8 mT of the undoped sample to 2.7 mT of the 8 % sample.

Both the effects of BCO on α and B^* can be explained with the properties of vortices. At low temperatures vortices are about the same size as BCO particles. Provided that the number of nanodots increase by increasing the concentration, like the number of nanorods in BZO doped YBCO [14], the behavior of B^* can be explained as there are more places for vortices with higher BCO concentration. However, near the critical temperature vortices are much larger than the BCO particles which makes the flux pinning much weaker. Also the additional defects created by BCO deteriorate the film quality. The undoped film has the best crystalline quality and that is seen as the highest T_c and the best J_c at self field and with the highest B^* near T_c .

C. The Angular Dependence of Critical Current

There are no major differences in the angular dependencies of critical current measured at 40 K and in the field of 6 T (Fig. 2) between the concentrations. The most notable change is that the peak around the case $B \parallel ab$ -axis ($\theta = \pm 90^\circ$) of YBCO (ab -peak) broadens as the BCO concentration increases. In practice, the curves measured at 10 K and at 40 K are very much alike, apart from the absolute value of J_c . However, at 70 K shoulders appear around the ab -peak. All in all, the peak widens as the measurement temperature is increased (Fig. 3 inset) and this effect is best seen near T_c . At higher temperature there are other pinning enhancements than mere BCO particles that are too small for vortices near T_c . However, in none of the samples, the typical c -axis peak for BZO doped YBCO (see [1], [3]) is seen. As can be expected, in the field of 1 T the ab -peak is much broader, because then the force acting on vortices is smaller.

One way to quantify the difference between the concentrations is to plot the ratio $I_{c,max}/I_{c,min}$ as a function of concentration at different measurement temperatures (Fig. 3). In the field of 6 T and far away from T_c , the ratio drops with increasing BCO concentration from 3.5 to 2.5 at 10 K

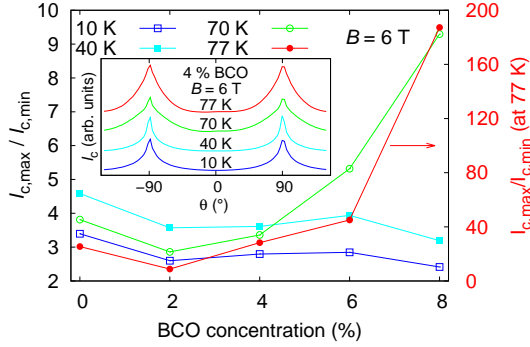


Fig. 3. The relation $I_{c,\max}/I_{c,\min}$ as a function of BCO concentration for measurement temperatures of 10, 40, 70 and 77 K. Please note that the scale for the 77 K data is on the right. The inset shows the evolution of $J_c(\theta)$ of the 4% doped sample in 6 T with different measurement temperatures. The curves have been normalized and shifted to emphasize the change of the shape.

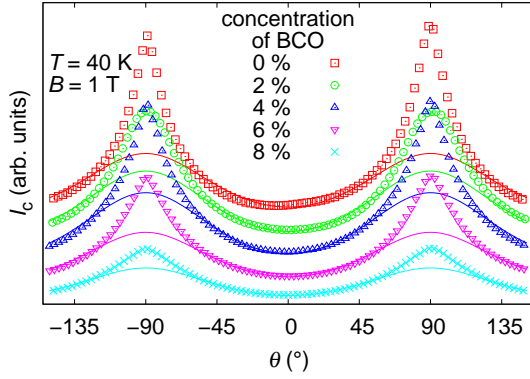


Fig. 4. The angular dependence of J_c as a function of angle between magnetic field and YBCO c -axis measured at 40 K and 1 T for different BCO concentrations. The solid lines are fits to Eq. (1). The curves have been shifted for clarity.

and from 5.5 to 3.5 at 40 K. At high temperatures the value rises, mainly because of the proximity of T_c especially with higher concentrations. The values calculated here are larger than the values of $I_c(90^\circ)/I_c(0^\circ)$ for BZO doped YBCO [19], mainly due to the lack of c -axis oriented correlated defects. On the other hand, for BZO doped films prepared with metal organic decomposition the ratio is much higher [22] than for BCO in this work. Again, in 1 T field the ratio is smaller, roughly between 1.3 and 2 for all the samples and measured temperatures without a clear correlation with concentration.

To more precisely describe the angular dependence, Blatter scaling in the form of Eq. (1) was fitted to the data at 40 K in 1 T. As a result, the function fits the data around $\theta = 0^\circ$ but near $\theta = 90^\circ$ it does not explain the behavior (Fig. 4), mainly because the clusters of BCO particles and stacking faults are both anisotropic defects. The $J_c(\theta)$ depends both on extrinsic and intrinsic properties of YBCO, and in practice it is difficult to determine the intrinsic parameter γ by measuring $J_c(\theta)$. Thus the γ in (1) can be considered as $\gamma_{\text{eff}}(\theta)$ and the fitted values are between 1.28 and 1.71 which is about the same as

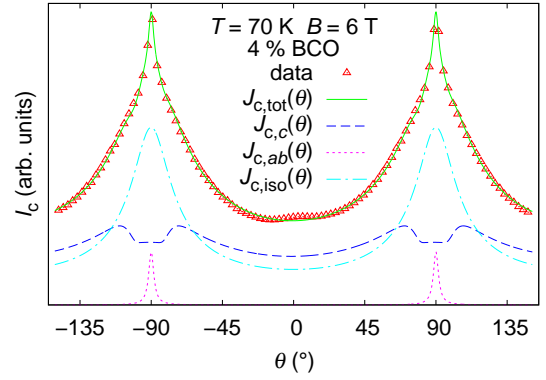


Fig. 5. Vortex path model fitted to 4% sample measured at 70 K and 6 T.

γ_{eff} for BZO doped films made by CSD [5] and by PLD [23].

The ab -peak in the data of 4% sample measured at 70 K in 6 T (data in Fig. 5) looks as if it is a result of two different pinning mechanisms. The point-like and partly clustered BCO particles improve pinning in rather wide angle in the case of $B||ab$ -axis of YBCO. In addition, the sharp peak is likely to be produced by the stacking faults also present in the sample.

To completely describe the anisotropic properties of $J_c(\theta)$, the vortex path model was fitted to that data (Fig. 5). The realization of the model is similar than in [19]. The model treats vortices in pinning centers statistically and the smaller is the variance of the steps taken by vortices, the narrower is the peak in $J_c(\theta)$. In addition to the Blatter scaling part, the model includes a Gaussian peak in the case $B||ab$ -axis of YBCO ($J_{c,ab}$) and a pseudo-Voigt peak as $B||c$ -axis of YBCO ($J_{c,c}$) and the total $J_c(\theta)$ is a sum of all three constituents. The anisotropy parameter γ was 5.0 in the fit since it intends to describe the intrinsic γ and it is higher than *e.g.* in FeAs-compounds [24], [25]. As the steps taken by vortices vary enough, the c -axis peak disappears and a contribution near ab -peak is seen, which is the case in BCO doped YBCO. Also, because the isotropic J_c is smaller than fitted in the mere Blatter scaling model, a part of J_c is due to anisotropic pinning, even in the case $B||c$ -axis of YBCO.

IV. CONCLUSIONS

YBCO thin films doped with 0 – 8 wt.% BCO were made by PLD. The BCO addition improves the in-field properties of J_c but with large concentrations degrades the crystal quality of YBCO considerably. This is seen for example as broadening of the YBCO (005) peak. Unlike BZO, BCO forms point-like, epitaxial, and partly correlated nanoparticles with diameter of 2.5 nm for 4% BCO sample. They broaden the ab -peak in $J_c(\theta)$ and no c -axis peak typical for BZO doped YBCO is seen. Although the particles are point-like, the data cannot be completely described with a model that only features isotropic pinning centers, which is partly because there are a lot of stacking faults in the samples. A model that describes also the anisotropic pinning centers, like the vortex path model, is needed to fully reconstruct the $J_c(\theta)$ curve.

REFERENCES

- [1] J. L. MacManus-Driscoll *et al.*, “Strongly enhanced current densities in superconducting coated conductors of $\text{YBa}_2\text{Cu}_3\text{O}_{7-x}+\text{BaZrO}_3$,” *Nat. Mater.*, vol. 3, pp. 439–443, 2004.
- [2] H. Yamada *et al.*, “Flux pinning properties of c-axis correlated pinning centres in PLD-YBCO films,” *Supercond. Sci. Technol.*, vol. 17, pp. S25–S29, 2004.
- [3] A. Goyal *et al.*, “Irradiation free, columnar defects comprised of self-assembled nanodots and nanorods resulting in strongly enhanced flux pinning in $\text{YBa}_2\text{Cu}_3\text{O}_{7-\delta}$ films,” *Supercond. Sci. Technol.*, vol. 18, pp. 1533–1538, 2005.
- [4] T. Puig *et al.*, “Vortex pinning in chemical solution nanostructured YBCO films,” *Supercond. Sci. Technol.*, vol. 21, p. 034008, 2008.
- [5] J. Gutiérrez, A. Llordés *et al.*, “Strong isotropic flux pinning in solution-derived $\text{YBa}_2\text{Cu}_3\text{O}_{7-x}$ nanocomposite superconducting films,” *Nat. Mater.*, vol. 6, pp. 367–373, 2007.
- [6] A. Llordés *et al.*, “Nanoscale strain-induced pair suppression as a vortex-pinning mechanism in high-temperature superconductors,” *Nat. Mater.*, vol. 11, pp. 329–336, 2012.
- [7] M. Irjala, H. Huhtinen, R. Jha, V. P. S. Awana, and P. Paturi, “Optimization of the BaCeO_3 concentration in YBCO films prepared by pulsed laser deposition,” *IEEE Trans. Appl. Supercond.*, vol. 21, pp. 2762–2766, 2011.
- [8] H. Palonen, H. Huhtinen, M. A. Shakhov, and P. Paturi, “Electron mass anisotropy of BaZrO_3 doped YBCO thin films in pulsed magnetic fields up to 30 T,” *Supercond. Sci. Technol.*, vol. 26, p. 045003, 2013.
- [9] G. Blatter, M. V. Feigel’man, V. B. Geshkenbein, A. I. Larkin, and V. M. Vinokur, “Vortices in high-temperature superconductors,” *Rev. Mod. Phys.*, vol. 66, pp. 1125–1388, 1994.
- [10] P. Paturi, “The vortex path model and angular dependence of J_c in thin YBCO films deposited from undoped and BaZrO_3 -doped targets,” *Supercond. Sci. Technol.*, vol. 23, p. 025030, 2010.
- [11] N. J. Long, N. M. Strickland, and E. F. Talantsev, “Modeling of vortex paths in HTS,” *IEEE Trans. Appl. Supercond.*, vol. 17, pp. 3684–3687, 2007.
- [12] N. J. Long, “Model for the angular dependence of critical currents in technical superconductors,” *Supercond. Sci. Technol.*, vol. 21, p. 025007, 2008.
- [13] S. Wimbush and N. Long, “The interpretation of the field angle dependence of the critical current in defect-engineered superconductors,” *New J. Phys.*, vol. 14, p. 083017, 2012.
- [14] P. Paturi, M. Irjala, H. Huhtinen, and A. B. Abrahamsen, “Modeling flux pinning in thin undoped and BaZrO_3 -doped YBCO films,” *J. Appl. Phys.*, vol. 105, p. 023904, 2009.
- [15] P. Paturi, M. Peurla, K. Nilsson, and J. Raittila, “Crystalline orientation and twin formation in YBCO thin films laser ablated from a nanocrystalline target,” *Supercond. Sci. Technol.*, vol. 17, pp. 564–570, 2004.
- [16] H. P. Wiesinger, F. M. Sauerzopf, and H. W. Weber, “On the calculation of J_c from magnetization measurements on superconductors,” *Physica C*, vol. 203, pp. 121–128, 1992.
- [17] J. H. Durrell, D. M. Feldmann, and C. Cantoni, “Suppression of vortex channeling in meandered $\text{YBa}_2\text{Cu}_3\text{O}_{7-\delta}$ grain boundaries,” *Appl. Phys. Lett.*, vol. 91, p. 182506, 2007.
- [18] A. Gauzzi and D. Pavuna, “Quantitative analysis of growth-induced reduction of long range lattice order in ion-beam sputtered $\text{YBa}_2\text{Cu}_3\text{O}_{6.9}$ films,” *Appl. Phys. Lett.*, vol. 66, pp. 1836–1838, 1995.
- [19] M. Malmivirta, L. Yao, H. Huhtinen, H. Palonen, S. van Dijken, and P. Paturi, “Three ranges of the angular dependence of critical current of BaZrO_3 doped $\text{YBa}_2\text{Cu}_3\text{O}_{7-\delta}$ thin films grown at different temperatures,” *Thin Solid Films*, vol. 562, pp. 554–560, 2014.
- [20] M. Peurla *et al.*, “Optimization of the BaZrO_3 concentration in YBCO films prepared by pulsed laser deposition,” *Supercond. Sci. Technol.*, vol. 19, pp. 767–771, 2006.
- [21] H. Huhtinen, H. Palonen, M. Malmivirta, R. Jha, V. P. S. Awana, and P. Paturi, “The effect of BaCeO_3 dopant concentration on magnetically defined B_{irr} and B_{c2} in $\text{YBa}_2\text{Cu}_3\text{O}_{6+x}$ thin films deposited on SrTiO_3 substrates,” *J. Phys. Conf. Ser.*, vol. 507, p. 012020, 2014.
- [22] A. Palau, A. Llordés, M. Gibert, T. Puig, A. Pomar, and X. Obradors, “Pinning landscape analysis in YBCO films with epitaxial and/or non-coherent BZO nanoparticles,” *IEEE Trans. Appl. Supercond.*, vol. 21, pp. 3243–3246, 2011.
- [23] P. Paturi, M. Irjala, and H. Huhtinen, “Greatly decreased critical current density anisotropy in $\text{YBa}_2\text{Cu}_3\text{O}_{6+x}$ thin films ablated from nanocrystalline and BaZrO_3 -doped nanocrystalline targets,” *J. Appl. Phys.*, vol. 103, p. 123907, 2008.
- [24] A. Yamamoto, J. Jaroszynski, C. Tarantini, L. Balicas, J. Jiang, A. Gurevich, D. C. Larbalestier, R. Jin, A. S. Sefat, M. McGuire, B. Sales, D. K. Christen, and D. Mandrus, “Small anisotropy, weak thermal fluctuations, and high field superconductivity in Co-doped iron pnictide $\text{Ba}(\text{Fe}_{1-x}\text{Co}_x)_2\text{As}_2$,” *Appl. Phys. Lett.*, vol. 94, p. 062511, 2009.
- [25] J. Kim, N. Haberkorn, K. Gofryk, M. J. Graf, L. Civale, F. Ronning, A. S. Sefat and R. Movshovich, “Intrinsic superconducting properties and vortex dynamics in heavily overdoped $\text{Ba}(\text{Fe}_{0.86}\text{Co}_{0.14})_2\text{As}_2$ single crystal,” *arXiv:1302.0074v1*, 2013.